Supporting Information

Kim and Warshel 10.1073/pnas.1324014111

SI Text

S1. Some Modeling Details

A crucial issue in modeling the effect of external potentials on membrane proteins is the proper modeling of the effect of the solvent molecules and the bulk ions. The solvent is modeled implicitly, but the ions in the solutions are considered more explicitly. That is, in trying to introduce the electrolytes, it is important to retain the option of multistage modeling by describing a key part of the system in a fully discrete model. For example, we can treat the immediate region near the protein by a primitive model with the explicit ions moving by Langevin dynamics treatment. Here, however, we have focused in our approach on the next layer of surrounding, where the electrolytes are described in a simpler way. This is done by adopting a compromise between full Monte Carlo (MC) and grid-type approaches. That is, we would like to start conceptually by placing ions on grid points (with an assumed separation) and then use an MC model of the type we and others applied in determining the ionization states in proteins. However, for practical purposes, we introduced some additional simplifications, which can also be removed. At any rate, we ended up with a semimacroscopic strategy applied in our previous electrostatic modeling, which is similar to the approach introduced originally by Pack and coworkers (1), but it retains a more microscopic view. In this approach, we generate a grid whose spacing is taken here as Δ with a volume element $\tau=\Delta^3$ and place at the center of the ith grid point a residual charge (q_i^g) determined by the following:

$$q_i^g = q_i^+ + q_i^-, \qquad \text{[S1]}$$

where

$$q_i^{\pm} = \frac{\alpha^{\pm}\left(N_{box}^{\pm}+N_{bulk}^{\pm}\right)e^{\mp\beta\phi_i}}{\left(\sum_{i\in box} e^{\mp\beta\phi_i}+N_{bulk}^{grid}e^{\mp\beta\phi_{bulk}}\right)}, \qquad \text{[S2]}$$

where q_i^+ and q_i^- are, respectively, the positive and negative fractional charges that are assigned to the ith grid point, $\alpha^{\pm}$ is the ion charge of the electrolyte ions in atomic units (namely, ± 1 for the 1:1 electrolyte used in our calculations), $N_{box}^{\pm}$ is the total number of cations/anions in the simulation box, $Q_{box}^{\pm}$ is the total charge of cations/anions in the simulation system given by $Q_{box}^{\pm}=\alpha^{\pm}N_{box}^{\pm}$, ϕ_i is the electrostatic potential (times a unit charge) at the ith grid point and $\beta=(k_BT)^{-1}$. N_{bulk}^{grid} is the number of grid points within the bulk system and ϕ_{bulk} is a constant potential on the bulk grid points (see ref. 2 for more details). ϕ_i can be expressed as follows:

$$\varphi_i = 332\sum_j \frac{q_j^P}{\varepsilon_{eff}^{gp} r_{ij}} + 332\sum_{k\neq i}\frac{q_k^g}{\varepsilon^{wat} r_{ik}} + V_i^{ext}, \qquad \text{[S3]}$$

where V_i^{ext} represents the external potential (time a unit charge) on the ith grid point that will be described below. Here, q_j^P is the charge of the jth protein residue (these charges are evaluated by MC procedure described above), and q_k^g is the point charge at the kth grid point (representing the excess net charge of the kth volume element). Eq. **S3** should also include the term $-RT\ln(C_i/C_0)$ due to the concentration dependence, in case of membrane potential with different concentration of electrolytes in the two sides of the membrane. The treatment of the boundary conditions is discussed in ref. 2. The final set of the grid charges (q_g) is obtained iteratively, and the effect of the ionic strength is evaluated as outlined in ref. 3.

To model the effect of the external potential, one can consider formally the membrane/protein/water system as a capacitor. In this case, it is possible to use the well-known macroscopic capacitor model (e.g., see ref. 4), where the external potential induces surface charges (σ_f) whose value will be defined below, and creates the corresponding displacement vector D^0. In this case, we have the following:

$$\mathbf{D}^0 = \sigma_f. \qquad \text{[S4]}$$

Our first task is to determine the membrane potential and the electrolyte charges, so we can evaluate the free energy of the protein charges in the presence of this potential. This is done by expressing the external potential as follows:

$$V_{ext}^i = \int_{Z_0}^{Z_i} D_z^0/\overline{\varepsilon}(Z)dZ, \qquad \text{[S5]}$$

where Z_0 is the Z coordinate at the left electrode (in the current work, we define the left side as side with smaller value for the Z coordinates and the right side with the larger Z value). The other alternative strategy is to replace the treatment of Eq. **S5** by simply having a finite grid of point charges on the electrode. Both treatments have been described and validated in ref. 3.

Our coarse-grained (CG) model describes the effect of the membrane head groups by electrostatic term with a high dielectric (see ref. 2). However, in the present study, we tuned this effect off, considering the fact the experimental finding of the important effect of theses head groups (5) should be left to more detailed subsequent studies that can also be used to validate and improve the representation of the head groups.

S2. The True Meaning of the Gating Charge

This gating charge concept was initially postulated by Hodgkin and Huxley (6) provides a qualitative explanation of the coupling of the external potential to the channel activation. The evaluation of the gating charge is usually done in an indirect way, using reasonable but not necessarily microscopic assumptions. This crucial issue is discussed in *SI Text*, section S2.

One may simply determine the relative population of open and closed channels as a function of the applied potential and determine the Boltzmann probability for the voltage-induced structural change. This is equivalent to the assumption that the energy needed to move the gating charge, Q_{gate}, in the applied electric field is equal to the work of moving the protein charges between the two configurations under the membrane electric field. This assumption can be formulated as follows:

$$Q_{gate}\Delta V = \Delta G^{cl\rightarrow op}, \qquad \text{[S6]}$$

where $\Delta G^{cl\rightarrow op}$ is the contribution of the membrane potential to the work of moving from the closed to open configuration, and ΔV is the change in the electrostatic potential between the initial and final position of the protein effective charge (for a case with many protein charges, see ref. 2). Under the assumption of linear membrane potential, it is simple to calculate Q_{gate} if the structures of the open and closed states are known and a useful

related insight has been obtained from macroscopic studies. Attempts to evaluate Q_{gate} from the equivalent of Eq. **1** using microscopic simulations have also been reported (e.g., see ref. 7). However, there are some problems with such strategies (see discussion in ref. 2, including the fact that the potential is not really linear or uniform in the protein membrane system (in contrast to the implicit assumption of one of the versions of the treatment of ref. 8). At any rate, we must consider the fact that the real observable is $\Delta G^{cl\rightarrow op}(V)$, which has not been obtained by microscopic simulation studies.

We would like to clarify that the results obtained with the linear approximation may well be very reasonable, but the fact that they reproduce the reasonably assumed gating charge should not be confused with the reproduction of a real observable. In fact, in view of the enormous importance of the gating charge and current, it is essential to strive for a model that obtains these quantities with an explicit description of the electrode/membrane and electrolytes instead of relying on a macroscopic concept that may be very elegant but as is the case with other problems with electrostatics in proteins (see discussion of different treatments of ref. 9) may lead to incorrect (and clearly unverifiable) conclusions.

S3. Structural Modeling

The full structural models of intermediate Kv1.2 (first, second, third, fourth, and fifth) were constructed by combining the structural models of voltage sensor domains (VSDs) from the *Shaker* channel (10) and of pore domains of Kv1.2 (11). Modeler (12) was used to build the full intermediate Kv1.2 structures based on the sequence alignment, taken from Long et al. (13), of the VSD from the *Shaker* channel and Kv1.2, whereas either the open or closed pore template from the K1.2v structures was used to construct the open model (the first state) or the rest of models that are closed (the second, third, fourth, and fifth states), respectively. Interdomain restraints between the pore and VSDs, derived from the structural alignment between Kv1.2 and VSD of the *Shaker* channel using align module implemented in Pymol, were incorporated into Modeler via Python interface to build the full models with correct orientation between the pore and VSDs. The structural models, constructed by Modeler, were subsequently refined using Rosetta membrane (14) with heavy atoms restraint of flat bottom potential with default width. The best model for each intermediate state was selected based on the standard Rosetta membrane environment scoring function (15). The final model for each intermediate state was then fed into the MOLARIS program (16, 17) to generate the corresponding CG model, followed by a molecular dynamics (MD) relaxation of 1 ps with the CG model of the protein and membrane. Finally, each pair of two intermediate states was used to locate the corresponding transition state structure. This was done by using a simple linear interpolation between two intermediate states, followed by a MD relaxation of 1 ps with the CG model.

Several key structural features of gating transitions of the VSD in the present model are consistent with a current consensus picture of voltage-sensing processes (18). The gating transitions involve sequential movements of positively charges residues in the S4 helix, which are stabilized by the negatively charged residues (E^{183}), (E^{226}, E^{236}), and (D^{259}) of the S1, S3, and S4 helixes, respectively. The modeled gating transitions, as is the case with the structural models of the VSD by ref. 10, involve predominant movements of the S4 helix along the relatively fixed S3 helix, sliding around 13 Å normal to membrane and rotating counterclockwise as viewed from the extracellular side, in accordance with the sliding-helix or helical-screw model (19, 20). The larger extension of a vertical moment of the S4 helix in the resulting model is different from the earlier structural model of Pathak et al. (11) with its smaller vertical movement of ~7 Å that supports the transporter model (see ref. 21 for review).

The model of the fifth state, which is suggested to exist in the paddle model (22), where R^{362} is stabilized in the gating charge transfer center (23) with an vertical movement of greater than ~15 Å, has been rejected in the present work, because its energetics was found to be much larger than at of first, second, third, and fourth. This state can still exist in a deep hyperpolarization state (10, 24).

1. Klein BJ, Pack GR (1983) Calculations of the spatial distribution of charge density in the environment of DNA. *Biopolymers* 22:2331–2352.
2. Dryga A, Chakrabarty S, Vicatos S, Warshel A (2012) Realistic simulation of the activation of voltage-gated ion channels. *Proc Natl Acad Sci USA* 109(9):3335–3340.
3. Dryga A, Chakrabarty S, Vicatos S, Warshel A (2012) Coarse grained model for exploring voltage dependent ion channels. *Biochim Biophys Acta* 1818(2):303–317.
4. Jackson JD (1998) *Classical Electrodynamics* (Wiley, New York).
5. Schmidt D, Jiang QX, MacKinnon R (2006) Phospholipids and the origin of cationic gating charges in voltage sensors. *Nature* 444(7120):775–779.
6. Hodgkin AL, Huxley AF (1952) A quantitative description of membrane current and its application to conduction and excitation in nerve. *J Physiol* 117(4):500–544.
7. Khalili-Araghi F, et al. (2010) Calculation of the gating charge for the Kv1.2 voltage-activated potassium channel. *Biophys J* 98(10):2189–2198.
8. Roux B (2008) The membrane potential and its representation by a constant electric field in computer simulations. *Biophys J* 95(9):4205–4216.
9. Warshel A, Sharma PK, Kato M, Parson WW (2006) Modeling electrostatic effects in proteins. *Biochim Biophys Acta* 1764(11):1647–1676.
10. Henrion U, et al. (2012) Tracking a complete voltage-sensor cycle with metal-ion bridges. *Proc Natl Acad Sci USA* 109(22):8552–8557.
11. Pathak MM, et al. (2007) Closing in on the resting state of the Shaker K^+ channel. *Neuron* 56(1):124–140.
12. Fiser A, Šali A (2003) Modeller: Generation and refinement of homology-based protein structure models. *Methods Enzymol* 374:461–491.
13. Long SB, Tao X, Campbell EB, MacKinnon R (2007) Atomic structure of a voltage-dependent K^+ channel in a lipid membrane-like environment. *Nature* 450(7168): 376–382.
14. Barth P, Wallner B, Baker D (2009) Prediction of membrane protein structures with complex topologies using limited constraints. *Proc Natl Acad Sci USA* 106(5):1409–1414.
15. Yarov-Yarovoy V, Baker D, Catterall WA (2006) Voltage sensor conformations in the open and closed states in ROSETTA structural models of K^+ channels. *Proc Natl Acad Sci USA* 103(19):7292–7297.
16. Lee FS, Chu ZT, Warshel A (1993) Microscopic and semimicroscopic calculations of electrostatic energies in proteins by the POLARIS and ENZYMIX programs. *J Comput Chem* 14(2):161–185.
17. Warshel A (2013) MOLARIS-XG: Theoretical background and practical examples. Available at http://laetro.usc.edu/programs/doc/theory_molaris_9.11.pdf.
18. Vargas E, et al. (2012) An emerging consensus on voltage-dependent gating from computational modeling and molecular dynamics simulations. *J Gen Physiol* 140(6): 587–594.
19. Catterall WA (1986) Voltage-dependent gating of sodium channels: Correlating structure and function. *Trends Neurosci* 9:7–10.
20. Guy HR, Seetharamulu P (1986) Molecular model of the action potential sodium channel. *Proc Natl Acad Sci USA* 83(2):508–512.
21. Bezanilla F (2002) Voltage sensor movements. *J Gen Physiol* 120(4):465–473.
22. Jiang Y, Ruta V, Chen J, Lee A, MacKinnon R (2003) The principle of gating charge movement in a voltage-dependent K^+ channel. *Nature* 423(6935):42–48.
23. Tao X, Lee A, Limapichat W, Dougherty DA, MacKinnon R (2010) A gating charge transfer center in voltage sensors. *Science* 328(5974):67–73.
24. Cole KS, Moore JW (1960) Potassium ion current in the squid giant axon: Dynamic characteristic. *Biophys J* 1:1–14.

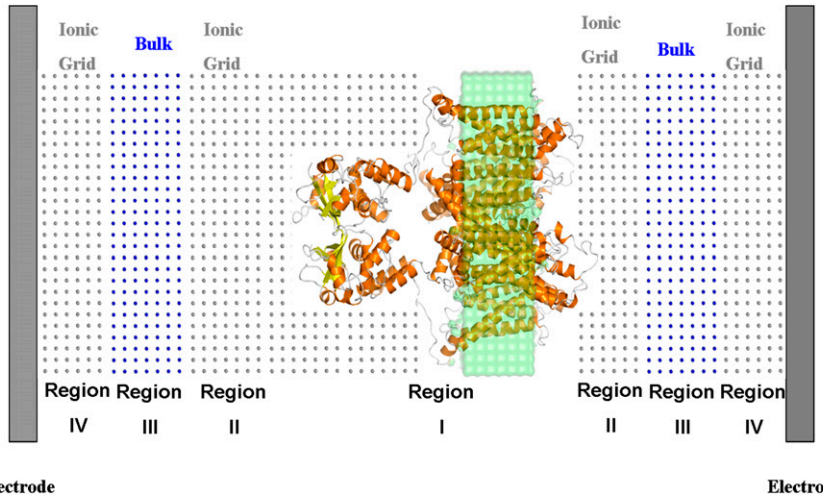

Fig. S1. A schematic description of the treatment of the simulation system. The regions considered are as follows: the protein/membrane system (region I); the region with explicit grid (region II); the bulk region (region III); and the region between the bulk and the electrodes (region IV). The "bulk region" far away from both the membrane and electrode surfaces provides as a specialized way for spanning the space between the membranes to the electrodes, without using an enormous grid.

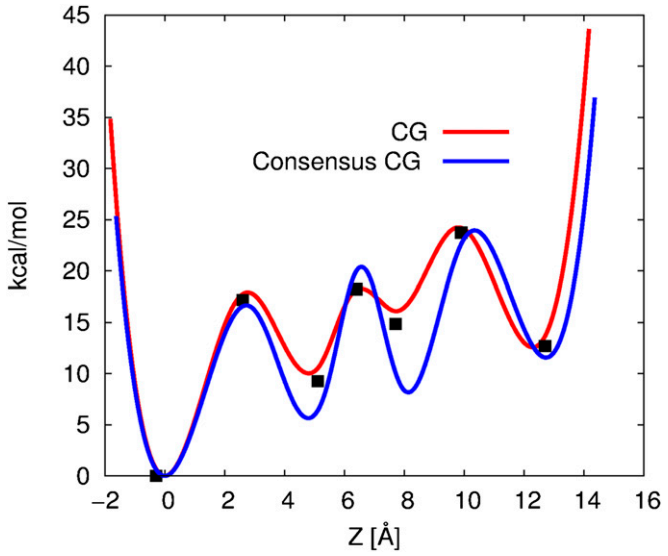

Fig. S2. Comparison between the actual CG free energy profile (red) with data points (filled square) and the consensus CG free energy profile (blue). The profiles of the CG and consensus surfaces were determined by the approach described in *Results and Discussion*, *The Energetics of the Activation Process*.

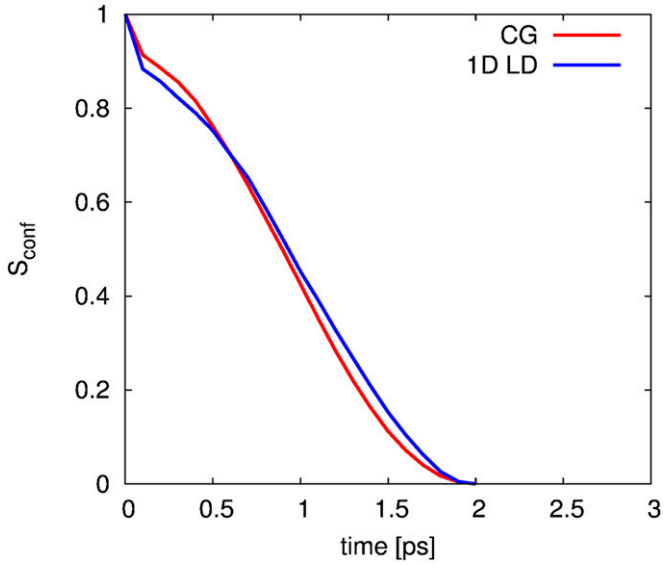

Fig. S3. The time response of the CG model and the reduced model (the 1D free energy surface) with an applied harmonic potential of the form $k(z - z_0)^2$, where k = 1 kcal/mol/Å^2 and z_0 = 8.5. S_{conf} (*y* axis) represents a fraction of the conformation transitions from the fourth (close) state to the third state.

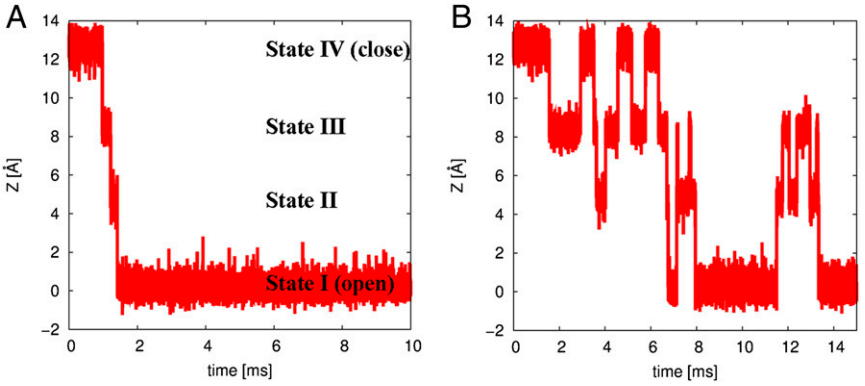

Fig. S4. The fluctuations of gating transitions at (*A*) 0 mV and (*B*) −50 mV: the simulations were done with a friction of 50 ps^{-1} (determined by a renormalization approach) on the unscale free energy surface (red curve in Fig. 3).

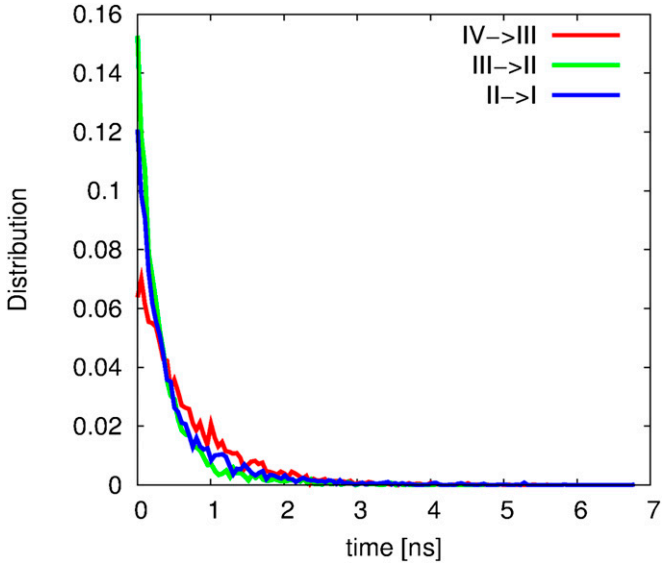

Fig. S5. The dwell time (or the first passage time) distributions for the conformational transitions between intermediate states at 0 mV: the average dwell times are 0.68, 0.40, and 0.53 ns (converted to the original timescale of 1.17, 2.41, and 7.00 ms) for the initial (red), second (green), and final (blue) transitions, respectively.

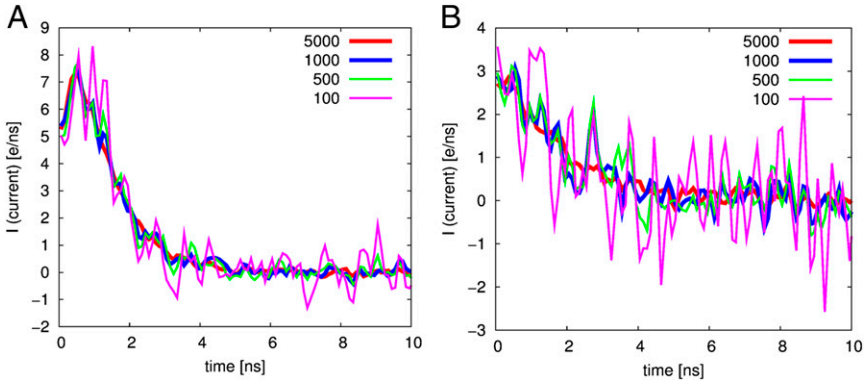

Fig. S6. The convergence profiles of the gating current at (*A*) 0 mV and (*B*) −50 mV: Langevin dynamics runs on the scaled free energy surface (red curve in Fig. 3) and the number of Langevin dynamics runs is given on the *Top Right*.

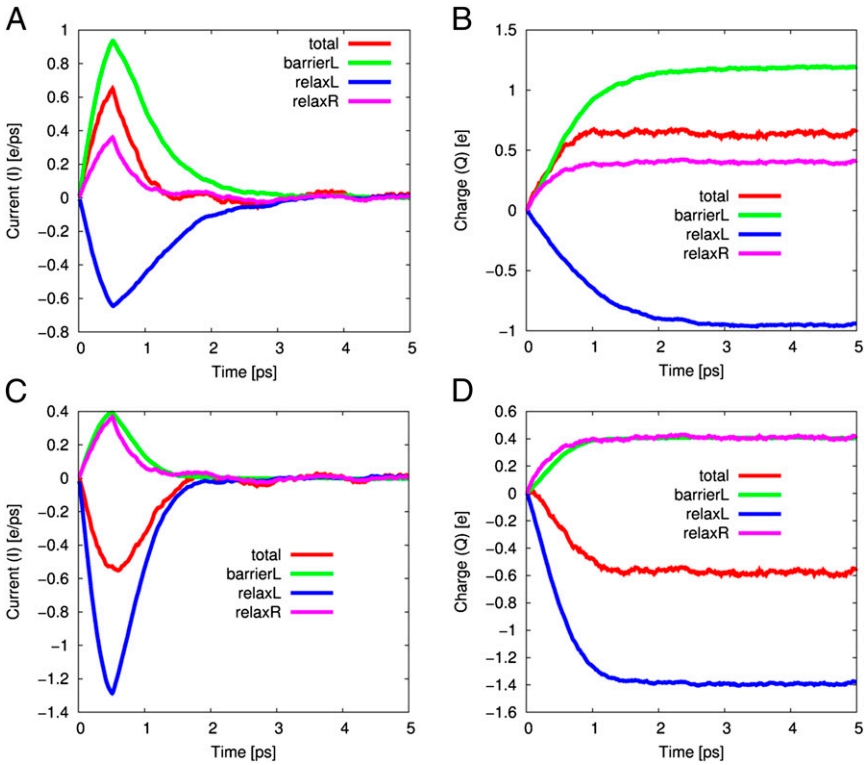

Fig. S7. The fast gating current and charge in response to changes in the membrane potential. (*A*) The total fast gating current (red curve) with (*B*) its corresponding gating charge, resulting from an increase in membrane potential from −50 to 0 mV. This current is predominantly determined by a barrier crossing contribution (green curve). (*C*) The total fast gating current (red curve) with (*D*) its corresponding gating charge, resulting from a drop from 0 to −50 mV in the membrane potential, is predominantly determined by a relaxation contribution (blue curve). Notice that the fast gating current contribution away from the closed state to the deeper state (purple curve) is considered small.

Table S1. The free energies (kcal/mol) of different intermediate states at low (−50 mV) and high (0 mV) depolarization

State\free energy	Protein electrostatics	Hydrophobic	Van der Waals	Hydrophilic	Electrolyte electrostatics	Total
State(IV) (close)						
Voltage, mV						
0	−100.97	−108.76	−15.04	14.63	27.69	−182.45
−50	−104.07	−110.76	−16.04	13.63	29.72	−187.52
Barrier for the (IV→III) transition						
Voltage, mV						
0	−91.71	−110.18	−15.51	14.57	31.43	−171.40
−50	−94.23	−111.17	−16.01	15.07	30.62	−175.72
State(III)						
Voltage, mV						
0	−103.92	−107.59	−16.00	14.52	32.70	−180.29
−50	−104.94	−111.59	−16.00	16.52	28.34	−187.67
Barrier for the (III→II) transition						
Voltage, mV						
0	−94.54	−110.47	−15.82	14.72	26.21	−176.90
−50	−95.05	−110.23	−15.72	16.22	29.21	−175.57
State(II)						
Voltage, mV						
0	−105.48	−106.37	−15.65	14.92	26.70	−185.88
−50	−104.85	−109.36	−15.65	15.92	26.08	−187.86
Barrier for the (II→I) transition						
Voltage, mV						
0	−94.79	−106.76	−15.72	12.32	27.02	−177.93
−50	−91.97	−108.23	−15.64	14.22	26.66	−174.96
State(I) (open)						
Voltage, mV						
0	−111.55	−105.63	−15.29	10.65	26.76	−195.13
−50	−106.24	−106.30	−15.23	12.38	28.79	−186.60